Structural and optical properties of Tb-doped Na–Gd metaphosphate glasses and glass-ceramics

2009 J. Phys.: Condens. Matter 21 155103

(http://iopscience.iop.org/0953-8984/21/15/155103)

J. Phys.: Condens. Matter **21** (2009) 155103 (7pp) doi:10.1088/0953-8984/21/15/155103

Structural and optical properties of Tb-doped Na–Gd metaphosphate glasses and glass-ceramics

F Moretti[1,3], A Vedda[1], M Nikl[2] and K Nitsch[2]

[1] Dipartimento di Scienza dei Materiali, Università di Milano-Bicocca, via Cozzi 53, 20125 Milano, Italy
[2] Institute of Physics AS CR, Cukrovarnicka 10, 162 00 Prague, Czech Republic

E-mail: federico.moretti@mater.unimib.it

Received 3 October 2008, in final form 22 January 2009
Published 17 March 2009
Online at stacks.iop.org/JPhysCM/21/155103

Abstract

The optical and structural properties of terbium doped sodium gadolinium phosphate glasses of three different compositions subjected to a crystallization process were studied and compared with those of the parent glassy samples. The structural characteristics of the glassy and crystallized phases were determined by Raman spectroscopy and the results showed a remarkable reduction in the full width at half maximum of the Raman peaks after crystallization. Radio-luminescence measurements revealed the emissions of both Gd^{3+} and Tb^{3+} ions. Their intensities strongly increased and their intensity ratio was modified by the crystallization. The luminescence temperature dependence investigated by radio-luminescence measurements in the temperature interval from 10 to 310 K became more complicated after crystallization. The role of free carrier trapping phenomena in the modification of the radio-luminescence efficiency was also studied by thermally stimulated luminescence.

(Some figures in this article are in colour only in the electronic version)

1. Introduction

Scintillators, materials capable of converting efficiently ionizing radiation into ultraviolet–visible (UV–vis) photons, are the subject of intensive research because of their wide possible applications from medical imaging and security control fields to high energy physics experimental apparatus [1].

The commonly used scintillators are in the form of single crystals which present high luminescence efficiency proper to highly ordered structures. However, the growth of large crystals with good optical and mechanical properties is often difficult and expensive. For this reason glass scintillators have been developed for those applications where large volume of the detectors is important and low production cost is an essential parameter. Other advantages of glassy scintillators with respect to crystalline ones are the compositional versatility and the easy shaping, including fibre drawing [2]. Unfortunately, glasses suffer from rather low scintillation efficiency [3] caused by defects present in the disordered glass matrix. These defects act as trapping sites and reduce the transfer of thermalized electrons and holes to the emitting centres. The trapping sites may also serve as non-radiative recombination channels contributing to the overall energy losses. A marked improvement of the scintillation efficiency of Ce^{3+}- and Tb^{3+}-doped phosphate glasses has recently been achieved by sufficiently increasing the concentration of Gd^{3+} ions in the glass samples [4, 5]. The Gd^{3+} ions act as luminescence sensitizers providing an efficient energy transfer channel toward the emitting Ce^{3+} or Tb^{3+} ions. This sensitization process is similar to that observed in some single crystalline matrices [6, 7]. The role of gadolinium concentration in optimizing the optical, scintillation, and structural properties of these phosphate glasses has recently been reported [8–10]. Thanks to the relatively low glass transition temperature of the studied glasses, information about their crystallization ability has also been obtained [11]. These results were particularly important because of the increasing interest in the synthesis and application of glass-ceramics scintillators.

[3] Author to whom any correspondence should be addressed.

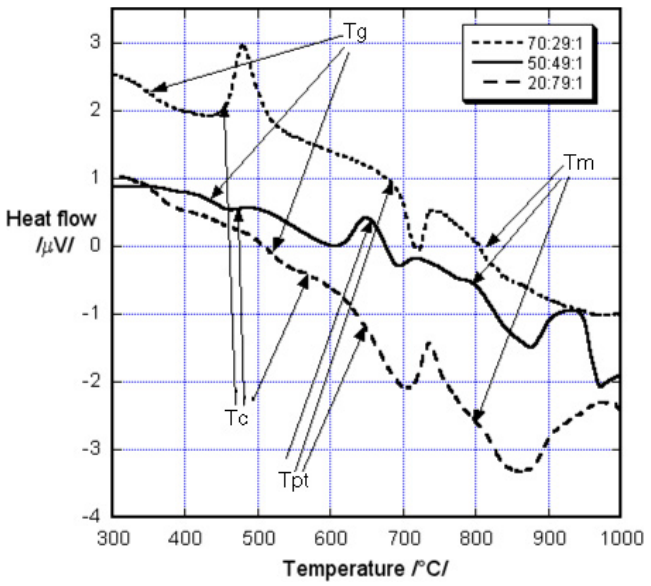

Figure 1. DSC curves of glass samples with nominal compositions of 70:29:1, 50:49:1 and 20:79:1. (T_g—temperature of glass transformation, T_c—crystallization temperature, T_m—melting temperature, T_{pt}—solid/solid phase transition.)

In this paper the results of our study of the optical and structural properties of Tb-doped sodium–gadolinium phosphate glasses subjected to a crystallization process are presented. These properties were studied by means of Raman scattering, radio-, thermo- and time-resolved photoluminescence measurements. Particular attention was paid to the direct comparison of the results obtained for the as-prepared glassy samples and those obtained for the crystallized ones.

2. Experimental conditions

Terbium doped sodium–gadolinium phosphate glasses were prepared by a rapid quenching technique using reagent grade $NaPO_3$, P_2O_5, $GdPO_4$ and $TbPO_4$. Three glass samples were prepared with different ratios of the starting components: 70:29:1, 50:49:1 and 20:79:1 where the figures denote the molar per cent concentration of Na, Gd and Tb phosphates. The same notation is used throughout this paper to specify the sample composition. The reagents in the required molar ratios with an excess of P_2O_5 compensating its evaporation during the preparation process were melted in a quartz crucible in air at 1200 °C. After homogenization the melt was cooled down by pouring it in a graphite mould which was preheated to a temperature of about 50 °C below the expected glass transition temperature. After a short tempering the ingot was cooled down to room temperature [5, 9]. The resulting glasses were transparent and colourless. The crystallized samples were prepared by keeping the glass samples above their glass transition temperatures from 15 to 90 days [11]. The typical dimensions of the samples were $1 \times 8 \times 8$ mm^3.

The thermal properties such as the temperatures of glass transition, crystallization, and melting were determined by differential scanning calorimetry (DSC) using a Setaram SETSYS Evolution 16 Thermal Analyzer. The characteristic temperatures were determined by using the software SETSOFT2000.

Table 1. Thermal properties and compositions of the studied glassy and crystalline samples. (T_g—temperature of glass transformation, T_c—crystallization temperature, T_m—melting temperature, X:Y:Z—molar concentration ratio between $NaPO_3$, $GdPO_4$ and $TbPO_4$ in the starting batch.)

Composition of glass (X:Y:Z)	T_g (°C)	T_c (°C)	T_m (°C)	Composition of glass-ceramics
70:29:1	357	457	810	$NaGd(PO_3)_4$
50:49:1	439	476	802	$NaGd(PO_3)_4$
20:79:1	516	560	800	$NaGd(PO_3)_4$-23 mol% $Gd(PO_3)_3$-22 mol% GdP_5O_{14}-55 mol%

The composition of the crystalline phases was determined from x-ray diffraction measurements using a Bruker D8 powder diffractometer. Raman measurements were performed at room temperature by a Labram Jobin-Yvon micro-Raman spectrometer using the internal He–Ne laser (632.8 nm) as excitation source. The unpolarized Raman spectra were collected in backscattering configuration through a CCD detector. Radio-luminescence (RL) was measured using a home-made apparatus working in the temperature range between 10 and 310 K and featuring a Jobin-Yvon Spectrum One 3000 CCD coupled to a Jobin-Yvon Triax 180 monochromator as detection system. RL excitation was obtained by x-ray irradiation through a beryllium window using a Philips 2274 x-ray tube with tungsten anode. Thermally stimulated luminescence (TSL) measurements were performed after x-ray irradiation at 10 K in the 10–310 K temperature interval with a heating rate of 0.1 K s^{-1} using the same apparatus employed in RL measurements. Photoluminescence (PL) time decay measurements were performed by a multichannel scaling technique under a microsecond Xe flash-lamp with an Edinburgh 199S spectrofluorometer.

3. Results and discussion

DSC curves of the studied glasses are shown in figure 1. Their thermal properties, namely the temperatures of glass transformation (T_g), crystallization (T_c) and melting (T_m), are summarized in table 1. All the three temperatures depend on glass composition: T_g and T_c clearly increase with Gd concentration in the glass; at variance, T_m slightly decreases. The compositions of the crystalline phases in individual ceramic samples, determined by x-ray diffraction, are also given in table 1. The diffraction patterns of 70:29:1 and 20:79:1 ceramic samples are shown in figure 2. In the 70:29:1 and 50:49:1 ceramic samples only the $NaGd(PO_3)_4$ crystalline phase was formed. Due to the low Na^+ ion concentration, in the 20:79:1 sample, besides the above mentioned $NaGd(PO_3)_4$, also sodium free crystalline phases such as $Gd(PO_3)_3$ and GdP_5O_{15} were formed. In the DSC curves there are also endothermic effects, indicated in figure 1 as T_{pt}, with onsets between 645 and 681 °C whose nature could not be precisely identified. They could reflect solid/solid phase transitions of the main component ($NaGd(PO_3)_4$) in the system. The

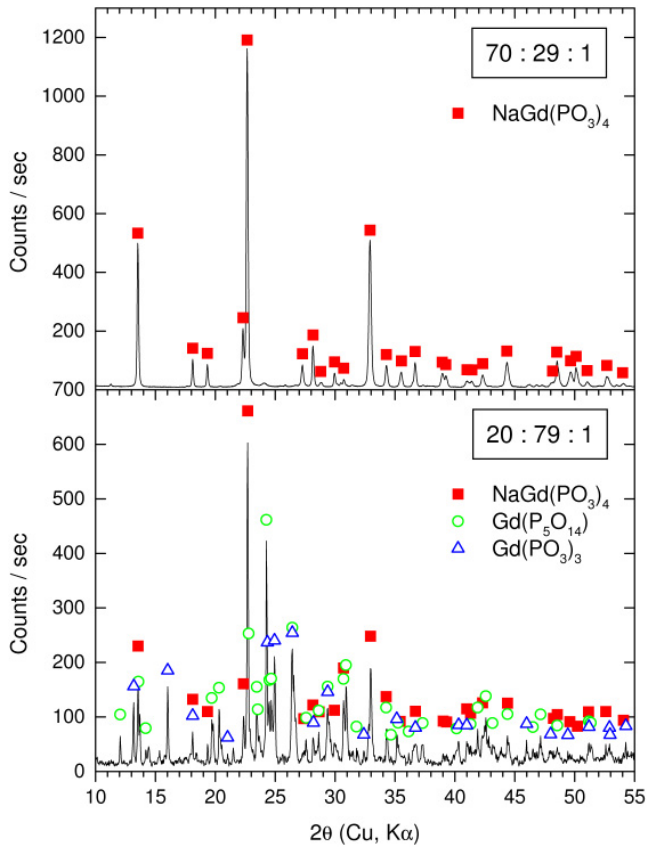

Figure 2. X-ray diffraction patterns of 70:29:1 and 20:79:1 glass-ceramics.

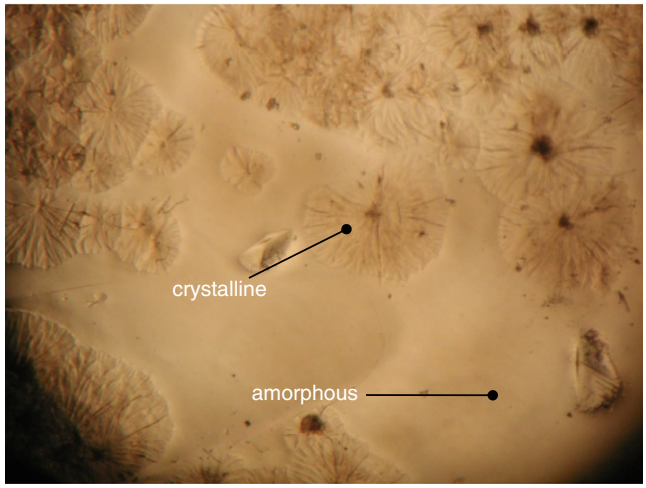

Figure 3. Micro-photograph of the crystallized 50:49:1 sample. Crystallized regions appear as flower-like areas, whose diameter is of the order of several hundreds of μm. The remaining glass is the surrounding unstructured region.

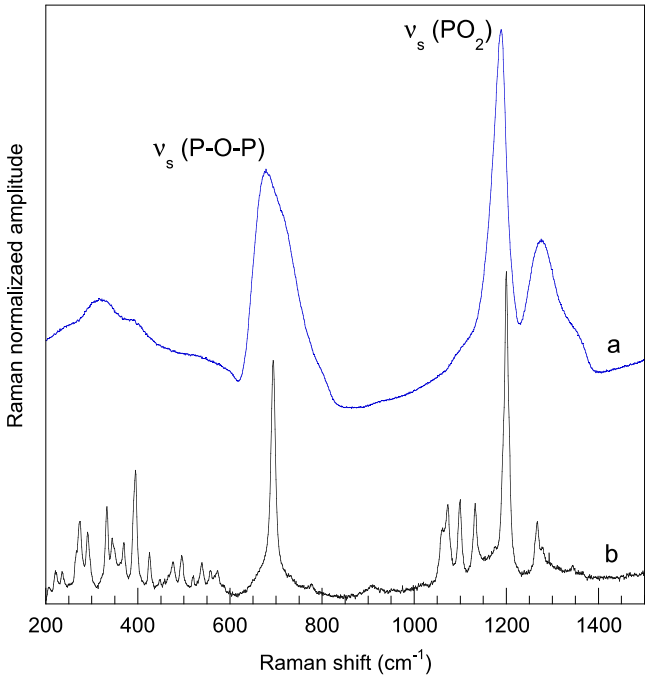

Figure 4. Room temperature Raman spectra of the 50:49:1 NaGdTb sample both before (a) and after (b) crystallization.

crystallized samples—glass-ceramics—were opaque due to many small crystallites arising in the glasses during the thermal treatment above the glass transition temperature. The crystallized parts, as well as the size and number of individual crystallites, depend on the treatment conditions. The content of crystallized phase represents about 30% of the overall volume. A nice structure, shown in figure 3, was observed with a microscope in the sample 50:49:1 treated at 465 °C for 21 days (nucleation) and at 478 °C for 21 days (crystallization). Crystallites look like flowers with a nucleus in their centres.

Raman spectra (reported in figure 4 for the 50:49:1 composition) of the glasses are characterized by two intense and broad peaks at about 700 and 1190 cm^{-1}, accompanied by other less intense structures between 1250 and 1370 cm^{-1} and in the low frequency (200–600 cm^{-1}) region. The common structural unit of phosphate glasses and crystals is PO_4 and the various possible condensations of this group result in several structural families [12, 13]: in the case of the investigated samples, the structure is characterized by long chains made by PO_4 tetrahedra each of which shares two corners (i.e. oxygens) with the others; the other two oxygens do not participate in the formation of the polyphosphate chains and remain as *non-bridging*. The 700 cm^{-1} Raman peak is related to the symmetric stretching of bridging oxygens (P–O–P) linking neighbouring PO_4 tetrahedra of the polyphosphate backbone, while the 1190 cm^{-1} band is assigned to the symmetric stretching of non-bridging oxygen (PO_2) on a PO_4 tetrahedron [14, 15]. According to literature results [14], the other structures are connected to bending and torsional vibrations of the polyphosphate backbone (300–400 cm^{-1}) and to (PO_2) asymmetric stretching (1250–1370 cm^{-1}). After the crystallization process, the full width at half maximum of the above mentioned bands is strongly reduced and sharper peaks appear where the glass spectra showed only broad and unstructured humps: the sharpening of all the Raman peaks clearly states the formation of crystalline phases. The spectra of 70:29:1 and 50:49:1 crystallized samples appear to be consistent with the literature results obtained on $NaGd(PO_3)_4$

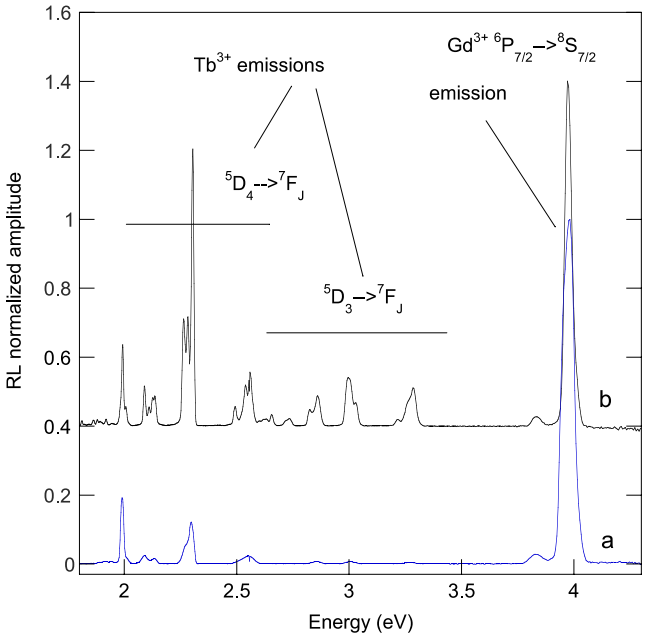

Figure 5. Normalized radio-luminescence spectra performed at 10 K on 50:49:1 NaGdTb samples before (a) and after (b) the crystallization process. The amplitudes were normalized to the maximum of the Gd^{3+} emission.

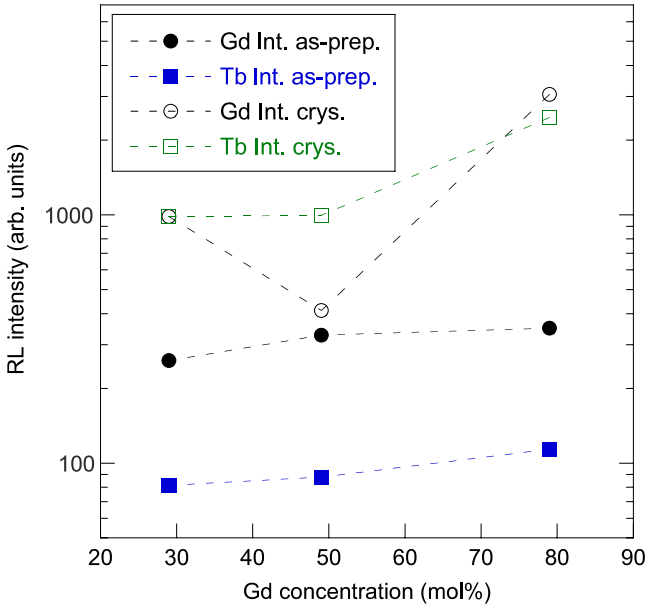

Figure 6. Room temperature RL intensities of Gd^{3+} and Tb^{3+} emissions, both before (full symbols) and after the crystallization (open symbols). The intensities are evaluated by integration of the spectra in the 3.70–4.13 eV and 2.00–3.54 eV intervals for Gd and Tb emissions, respectively.

single crystals [16]. However, a different Raman spectrum characterizes the highest gadolinium containing crystallized sample: the observed differences can be related to the formation of the two gadolinium rich phases evidenced by the x-ray diffraction (XRD) results. Moreover, it is worth noticing that Raman spectra obtained in the non-crystallized regions of the samples are almost identical to that of the parent glasses.

RL measurements (figure 5, where the spectra obtained at 10 K on both as-prepared and crystallized 50:49:1 NaGdTb phosphate samples are reported as an example) are characterized by a series of narrow emission lines in the blue–green region of the spectrum (2.0–3.5 eV interval), due to the Tb^{3+} transitions from the $^5D_4$ and $^5D_3$ terms to the ^7F_J ground levels, and a more intense one at about 3.98 eV related to the Gd^{3+} $^6P_{7/2}$–$^8S_{7/2}$ transition [17]. This latter emission line is accompanied by a less intense band centred at about 3.84 eV, which can be assigned to the phononic replica of the $^6P_{7/2}$–$^8S_{7/2}Gd^{3+}$ transition [18]. In fact, the energy difference between the 3.84 eV band and the Gd^{3+} main emission is about 1140 cm^{-1} (0.14 eV). Considering the wavelength precision of the RL apparatus, this value is in accordance with the energy of the PO_2 vibration of the phosphate structure obtained by Raman measurements. The modifications of the RL spectrum shape induced by crystallization can be easily observed in figure 3. In particular, it is worth noticing that the amplitude of the Tb^{3+} emissions is increased with respect to that of Gd^{3+}; moreover, there is also an evident modification in the intensity ratio among the $^5D_4$–^7F_J and $^5D_3$–^7F_J Tb^{3+} emissions, since the latter clearly increase more after crystallization. Furthermore, especially at low temperature, all the emissions are narrower and more structured because of the reduction of the inhomogeneous broadening in the crystallized regions. The intensity ratio between the $^5D_4$–^7F_J and $^5D_3$–^7F_J peak groups depends on the probability of cross relaxation among Tb^{3+} ions [17, 19, 20], which is in turn strongly influenced by the distance between them: the achieved results point to a better dispersion and a larger mean distance among terbium ions in the crystalline region, induced by the crystallization process, with respect to as-prepared glass samples, so reducing the cross relaxation probability and favouring the luminescence starting from the $^5D_3$ levels.

In figure 6 the RL intensities of Gd^{3+} and Tb^{3+} emissions (obtained by integration of the spectra in the 3.70–4.13 eV and 2.00–3.54 eV intervals for Gd^{3+} and Tb^{3+} emissions, respectively) are presented as a function of Gd concentration both before and after crystallization. As is clearly visible, for all the considered compositions the Gd^{3+} intensities in the as-prepared samples are about three times higher than those of Tb^{3+}. Moreover, both Gd and Tb intensities slightly increase by increasing gadolinium concentration: this increment is more pronounced for the Tb emissions than for the Gd one. After the crystallization, all the intensities are strongly enhanced with the only exception being the gadolinium emission of the 50:49:1 sample. Furthermore, the Tb^{3+} emission intensities appear comparable with, and in the case of 50:49:1 higher than, the Gd^{3+} ones. Also in this case, the Tb^{3+} intensity increases slightly with gadolinium concentration. Such an increase could be related to a higher probability of energy transfer (ET) phenomena among gadolinium ions toward Tb^{3+}, induced by a smaller distance among gadolinium ions. An increased ET probability after the crystallization could explain why Tb intensities are more effectively increased by the crystallization process, becoming comparable to those of Gd: as a matter of fact lower fluctuation in the geometry of RE hosting sites

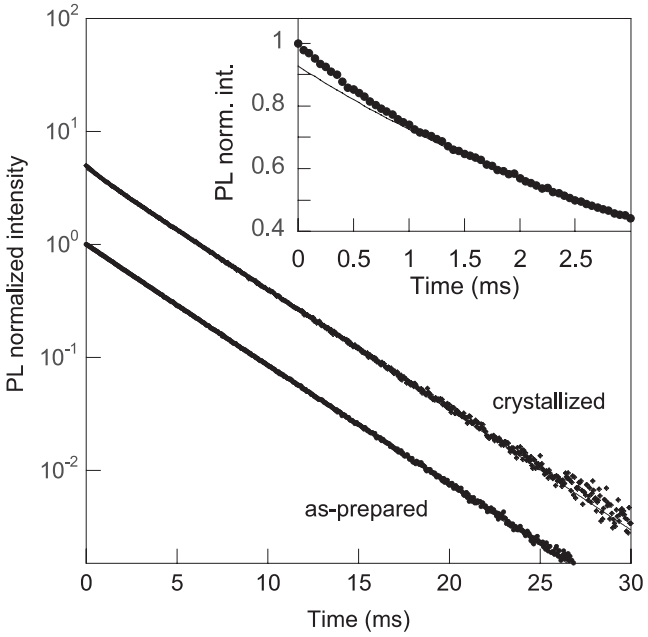

Figure 7. PL decay course of the Gd emission ($E_{exc} = 4.50$ eV, $E_{em} = 3.97$ eV) of 50:49:1 NaGdTb phosphate before and after crystallization. Inset: enlargements of the first 3 ms Gd^{3+} decay of the re-crystallized sample (symbols) and its approximation in terms of a single exponential decay (full line).

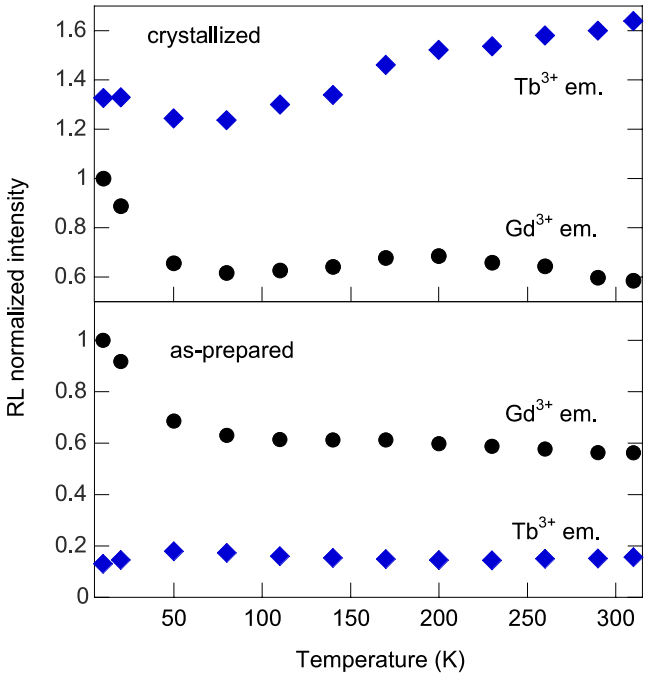

Figure 8. Normalized RL intensities versus temperature of Gd^{3+} and Tb^{3+} emissions before and after crystallization of 50:49:1 samples. The RL intensities were obtained after integration of the spectra in the 3.70–4.13 eV and 2.00–3.54 eV intervals for Gd^{3+} and Tb^{3+} emissions, respectively, and normalized to the Gd^{3+} emission values at 10 K.

should favour the excitation transfer through the gadolinium sublattice toward the Tb^{3+} emitting centres.

In order to verify this hypothesis, photo-luminescence time decay measurements (PL) monitoring the Gd^{3+} emission ($E_{exc} = 4.5$ eV, $E_{em} = 3.97$ eV) were carried out. These measurements (figure 7), performed on 50:49:1 samples both before and after crystallization, showed that the Gd^{3+} decay is not considerably affected by the crystallization process since it can be described by a single exponential component with the same decay time (of about 4.08 ms) for both amorphous and crystallized samples. The only variation in the decay observed after the crystallization is represented by the decay acceleration in the first 2 ms (inset of figure 7). Integrating the normalized decays from the amorphous and crystallized samples it is estimated that only about 5% of the overall Gd^{3+} emission intensity could be additionally transferred out of the Gd-sublattice in the latter case. An increased energy transfer probability among Gd^{3+} ions, able to strongly increase the Tb^{3+}–Gd^{3+} intensity ratio, should result in a notable modification of the gadolinium decay course either by lowering the decay time or by presenting a notable acceleration in the initial decay part [21, 22]: since PL decay measurements did not show such pronounced modifications, other factors must be considered in order to explain the higher Tb^{3+}/Gd^{3+} intensity ratio after the crystallization. Since all the RL emissions of the re-crystallized samples are narrower and more structured than those of the as-prepared ones, it appears that the spectra of the crystallized samples are dominated by the luminescence coming from the crystalline regions. So, it is possible that the strong luminescence intensity increase could be due to the disappearance of non-radiative recombination channels, resulting in more efficient excitation of emitting centres.

In figure 8 the temperature dependence of the Gd^{3+} and Tb^{3+} emission intensities, normalized at the 10 K Gd^{3+} value, is presented for the 50:49:1 sample both before and after crystallization. As can be clearly seen, for the as-prepared sample the Gd^{3+} emission intensity has its maximum value at 10 K where the Tb^{3+} one has its lowest value. By raising the temperature, the gadolinium intensity decreases, losing about 40% of its initial value in the first 70 K; above this temperature, the Gd^{3+} intensity still decreases but at a far lower rate. The Tb^{3+} intensity increases by temperature increasing up to about 70 K, while above this temperature it does not change appreciably. After crystallization both Gd and Tb emissions present a more complex temperature dependence: the Tb and Gd emission intensities decrease by raising the temperature and reach their minima at about 70 K. Above this temperature the Tb intensity increases steadily up to room temperature, while the Gd emission intensity increases slightly up to 200 K and then decreases for higher temperatures.

In order to clarify the role of free carrier trapping phenomena on the temperature dependence of RL intensities, TSL measurements were performed on as-prepared and crystallized samples. In figure 9 the glow curves are presented for all the crystallized and one glass samples obtained after integration of wavelength resolved measurements in the 2.07–3.50 eV interval. The TSL glow curves of the glasses are similar and are characterized by a monotonically decreasing signal in the 10–100 K interval, possibly related to a thermal tunnelling emission [23]; above this temperature no other

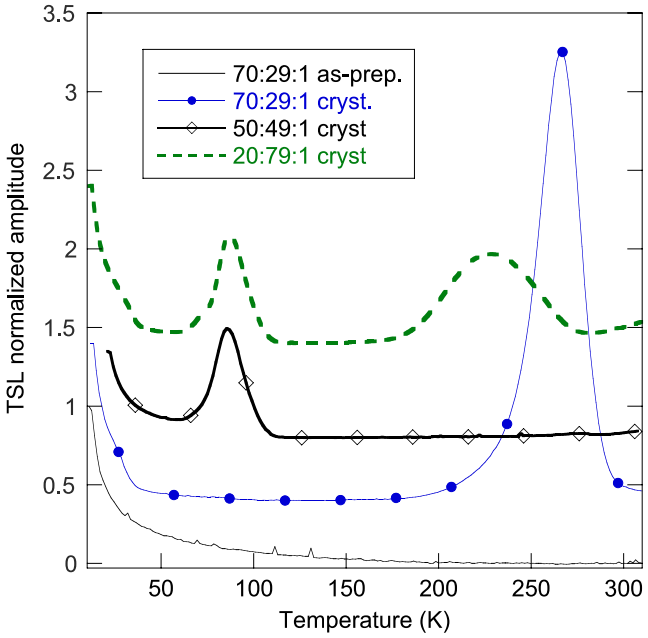

Figure 9. TSL glow curves of NaGdTb phosphate samples obtained after integration of wavelength resolved measurements in the 2.07–3.50 eV emission interval.

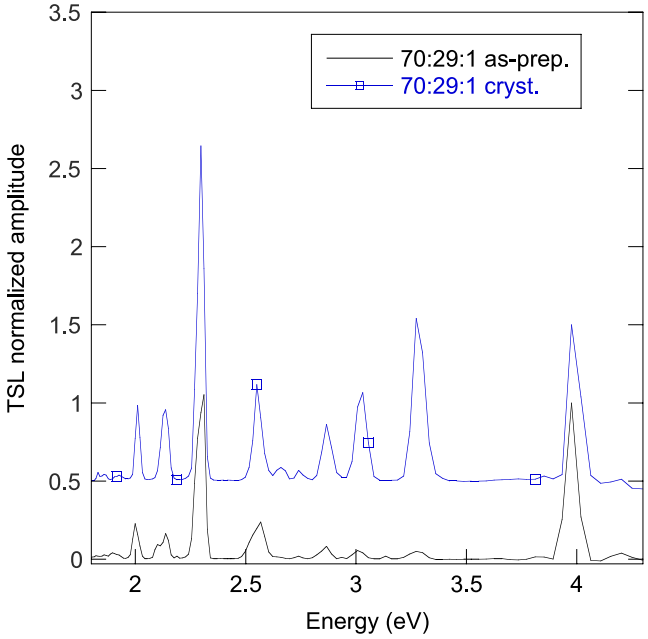

Figure 10. TSL spectra obtained after integration of wavelength resolved TSL measurements of amorphous (integral between 12 and 80 K) and crystallized (integral between 200 and 310 K) 70:29:1 NaGdTb phosphate samples.

structures were detected. The crystallized samples also present this decreasing signal, clearly visible in the 10–40 K interval, together with glow peaks whose characteristics depend on the sample composition, and that are possibly related to the crystallized regions. The 20:79:1 sample showed two glow peaks at about 90 and 230 K, while the 50:49:1 sample showed only that at 90 K. The glow curve of the 70:29:1 sample is characterized by a single peak at about 260 K. TSL emission spectra, reported in figure 10, showed that the carrier recombination takes place on both Gd^{3+} and Tb^{3+} ions. Recombination at Tb^{3+} ions is more probable since the Tb^{3+} intensities are larger than those of Gd^{3+} (with the only exception of the 20:79:1 crystallized sample). Moreover, as observed in the RL measurements, the ratio among $^5D_4$–^7F_J and $^5D_3$–^7F_J Tb^{3+} emissions is modified by the crystallization.

The temperature dependences of Gd^{3+} and Tb^{3+} emissions can be discussed also taking into account the above described trapping phenomena. The decreasing Gd^{3+} emission intensities observed by raising the temperature from 10 up to 70 K, for both glass and crystallized samples could be related to energy transfer (ET) phenomena. We showed that ET processes are not responsible for the increase of the Tb^{3+}/Gd^{3+} emission intensity ratio at room temperature after crystallization. However, it is possible that they are evidenced to some extent at low enough temperatures: since they could be thermally assisted, they could give rise to the observed decrease of Gd^{3+} emission from 10 to 70 K. As temperature is raised, in fact, the excitation can be more easily transferred among Gd ions in multiple steps until it finds a recombination channel, both radiative and non-radiative, resulting in the partial quenching of the Gd^{3+} luminescence. Above 70 K, the energy transfer probability becomes much less temperature-dependent, leading to almost constant Gd^{3+} and Tb^{3+} intensities. Similar PL results were recently obtained in photo-luminescence measurements of the same kind of glasses doped with other rare earths and transition metal ions [22].

Despite the more complex temperature dependence, the just reported situation is still valid for the crystallized sample, accounting for both the decrease of the Gd^{3+} emission intensity and the increase of the Tb^{3+} one. However, the different behaviour in the 30–120 K interval must be explained by considering other factors, like the presence of competitive processes related to the traps responsible for the TSL glow peak at about 90 K. As a matter of fact, besides the prompt RL recombination, carriers can also be trapped at localized levels whose stability depends on temperature. Since the detrapping probability below 70 K is negligible, carriers trapped on such states cannot participate in the RL recombination processes; at higher temperatures, the detrapping becomes more and more probable leading to a higher number of carriers available for the RL recombination. So, there are two processes, namely the ET and trapping phenomena (each of these with its own temperature dependence), which participate in shaping the temperature dependences of Gd and Tb radio-luminescence emission intensities. Moreover, we cannot exclude that also the decreasing TSL signal observed on both as-prepared and crystallized samples in the 10–70 K interval could have a role in the RL intensity temperature dependence. However, from a qualitative comparison between RL and phosphorescence intensities, we estimate that such a contribution should not exceed a few per cent of the total RL signal.

4. Conclusions

Tb-doped NaGd phosphate glasses with three different Na:Gd ratios were prepared by a rapid quenching technique of the melt. The temperatures of glass transformation, crystallization and melting were determined with a DSC technique; the two former show distinct increase with Gd content. The optical and structural properties of Tb-doped NaGd phosphate glass are modified by thermal treatments which induce a partial crystallization of the samples. In the glasses with an Na:Gd molar ratio greater than one the crystallized phase is purely $NaGd(PO_3)_4$, while in the glass with the highest concentration of Gd two other Gd-rich crystalline phases were found by XRD, namely $Gd(PO_3)_3$ and GdP_5O_{15}. The formation of crystalline micro-phases is reflected in a narrowing of the Raman features. Furthermore, it is directly connected to the increase of the radio-luminescence intensity and to the change of the Tb^{3+}/Gd^{3+} emission intensity ratio. This intensity ratio modification is not related to an increased probability of energy transfer from gadolinium to terbium ions, since the Gd^{3+} PL decay curve is not remarkably affected by crystallization. Rather, the disappearance of non-radiative channels and the modification of charge carrier capture by Gd^{3+} and Tb^{3+} ions in the crystalline micro-regions can be suggested. The more complex temperature dependence of the RL intensity observed after crystallization is related to carrier trapping at defect sites, whose characteristics were studied by TSL measurements.

Acknowledgments

The authors gratefully acknowledge the financial support of the Italian Cariplo Foundation Project 'Structure and optical properties of self-organized nano and mesoscopic materials' (2006–2008) and the Grant Agency of the Academy of Sciences of the Czech Republic (No. IAA200100626). Thanks are given to K Knizek and M Rodova from the Institute of Physics AS CR for XRD and DSC measurements, respectively.

References

[1] Rodnyi P 1997 *Physical Processes in Inorganic Scintillators* (New York: CRC Press)
[2] Vedda A, Chiodini N, Di Martino D, Fasoli M, Keffer S, Lauria A, Martini M, Moretti F and Spinolo G 2004 *Appl. Phys. Lett.* **85** 6356–8
[3] Auffray E *et al* 1996 *Nucl. Instrum. Methods Phys. Res.* A **380** 524–36
[4] Nikl M, Nitsch K, Mihokova E, Solovieva N, Mares J A, Fabeni P, Pazzi G P, Martini M, Vedda A and Baccaro S 2000 *Appl. Phys. Lett.* **77** 2159–61
[5] Rodová M, Cihlář A, Knížek K, Nitsch K and Solovieva N 2004 *Radiat. Meas.* **38** 489–92
[6] Blasse G 1993 *J. Alloys Compounds* **192** 17–21
[7] Mares J A, Nikl M, Mihokova E, Kvapil J, Giba J and Blazek K 1997 *J. Lumin.* **72–74** 737–9
[8] Mares J A, Nikl M, Nitsch K, Solovieva N, Krasnikov A and Zazubovich S 2001 *J. Lumin.* **94/95** 321–4
[9] Nikl M *et al* 2001 *Radiat. Meas.* **33** 593–6
[10] Nitsch K, Cihlář A, Klimm D, Nikl M and Rodová M 2005 *J. Therm. Anal. Calorim.* **80** 735–8
[11] Nitsch K and Rodová M 2008 *J. Therm. Anal. Calorim.* **91** 137–40
[12] Rekik W, Naili H and Mhiri T 2004 *Acta Crystallogr.* C **60** i50-2
[13] Dinh C T, Huong P V, Olazcuaga R and Fouassier C 2000 *J. Optoelectron. Adv. Mater.* **2** 159–69
[14] Hudgens J J, Brow R K, Tallant D R and Martin S W 1998 *J. Non-Cryst. Solids* **223** 21–31
[15] Nelson B N and Exarhos G J 1979 *J. Chem. Phys.* **71** 2739–47
[16] Amami J, Férid and Trabelsi-Ayedi M 2005 *Mater. Res. Bull.* **40** 2144–52
[17] Blasse G and Grabmaier B C 1994 *Luminescent Materials* (Berlin: Springer)
[18] Di Martino D, Krasnikov A, Nikl M, Nitsch K, Vedda A and Zazubovich S 2004 *Phys. Status Solidi* a **201** R38–40
[19] Pucker G, Praolin S, Moser E, Montagna M, Ferrari M and Del Long L 1998 *Spectrochim. Acta* A **54** 2133–42
[20] Armellini C, Ferrari F, Montagna M, Pucker G, Bernard C and Monteil A 1999 *J. Non-Cryst. Solids* **245** 115–21
[21] Solovieva N, Nikl M and Nitsch K 2007 *Opt. Mater.* **30** 113–5
[22] Babin V, Krasnikov A, Mares J A, Nikl M, Nitsch K, Solovieva N and Zazubovich S 2003 *Phys. Status Solidi* a **196** 484–95
[23] Fasoli M, Fontana I, Moretti F, Vedda A, Nikl M, Mihokiva E, Zorenko Y V and Gorbenko V I 2008 *IEEE Trans. Nucl. Sci.* **55** 1114–7